Supporting Information

Flexible Polydimethylsilane Nanocomposites Enhanced with a Three-Dimensional Graphene/Carbon Nanotube Bicontinuous Framework for High-Performance Electromagnetic Interference Shielding

Sumin Zhao, Yehai Yan, Ailin Gao, Shuai Zhao, Jian Cui, and Guangfa Zhang*

Key Laboratory of Rubber-Plastics, Ministry of Education/Shandong Provincial Key Laboratory of Rubber-Plastics, School of Polymer Science and Engineering, Qingdao University of Science and Technology, Qingdao 266042, P. R. China

AUTHOR INFORMATION

Corresponding Author

E-mail: gfzhang@qust.edu.cn (G. Zhang)

Synthesis of graphene oxides (GOs)

GOs were synthesized by a modified Hummers method. In a typical process, graphite powder (1.0 g) was added to concentrated H_2SO_4 (23 mL) under magnetic stirring in an ice bath. After the graphite was well dispersed, $KMnO_4$ (3.0 g) was added slowly to ensure the temperature of the solution lower than 20 °C. Successively, the reaction system was transferred to a 45 °C oil bath and stirred vigorously for 2 h. Then, 50 mL ultrapure (UP) water was added into the mixture, and the solution was stirred for another 15 min at 95 °C. Additional 160 mL UP water was subsequently added and followed by a slow addition of 5 mL H_2O_2 (30%), turning the color of the solution from dark brown to golden yellow. The mixture was washed with 1:10 HCl aqueous solution (80 mL) for three times to remove residual metal ions, and further washed with plenty of UP water and dialyzed for one week to eliminate remaining acidic impurities. The resultant graphite oxide aqueous dispersion with a concentration of ~12 mg/ml was sonicated for 60 min to exfoliate it to GO. Finally, the GO dispersion was then centrifuged at 4000 rpm for 40 min to remove the unexfoliated graphite, yielding the pure GO aqueous dispersion.

The GO morphology features was also measured by AFM. As shown in **Figure S1**, the thickness of as-obtained GO sheets is around 1.1 nm, indicating the successful preparation of single-layered GO in this work. Besides, the lateral lengths of most GO sheets is less than 1μm due to the efficient mixing process.

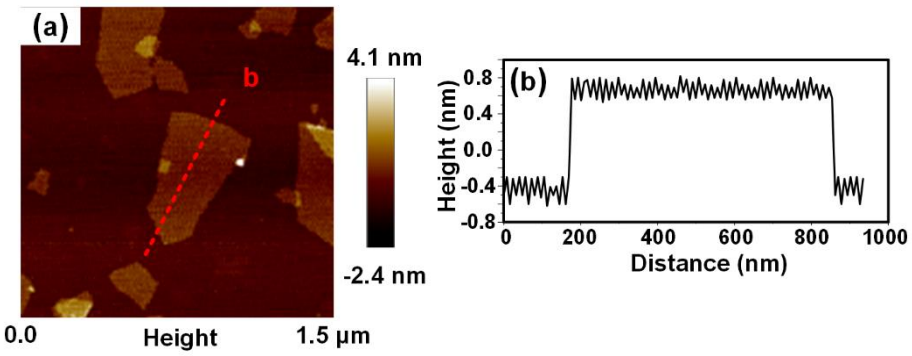

Figure S1. AFM height image (a), and height profile of GO (b).

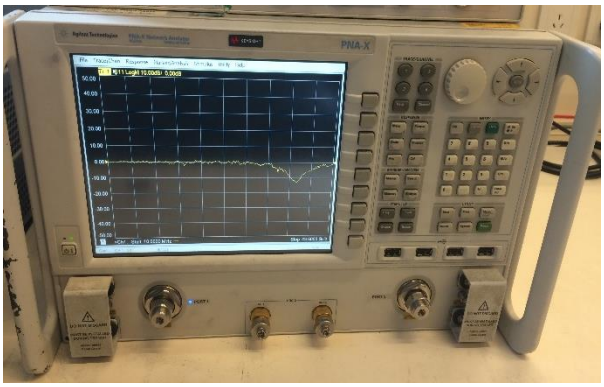

Figure S2. Experiment apparatus (vector network analyzer) for EMI shielding measurement.

Cyclic compression performance of TGCAs and PTGCAs

As shown in **Figure S 3(a)**, cyclic compression test of TGCA3 aerogel with 10 cycles have been performed under a maximum strain of 78%. For the first cycle, there is a steep increase in the stress-strain curve of the aerogel, which corresponded to a densification region due to the successively decreasing pore volume accompanied with the close stacking of its cellular structure. Interestingly, the TGCA3 aerogel achieve a maximal compression stress of around 3.3 kPa at the maximum strain of 78%. Compared with the first cycle, the hysteresis loop of the second cycle exhibits a smaller shrink, whereas no apparent enhancement in shrink for the stress-strain curves is observed from the third to tenth cycles. Meanwhile, there is no obvious decline in the maximum compressive stress of TGCA3 aerogel during the cyclic test. Additionally, the cyclic compressive testing of TGCA3 aerogel for 20 cycles of the compressing-recovering process at the strain of 60% is also examined, as illustrated in **Figure S 3(b)**. Small shrink in the stress-strain curve is clearly observed after the first cycle, but only tiny shrink is found in the second to twentieth cycles. Besides, the maximum compressive stress of aerogels during the whole cyclic test show a quite tiny decrease. Therefore, our prepared aerogels display outstanding compressibility and super-elasticity, thus providing them excellent application functionalities, such as superior mechanical stability, good recyclability as an absorbent material, and variable electrical resistance.

On the other hand, for comparison, the cyclic compression performance of PDMS-infiltrated aerogel, i.e., PTGCA3 composite, has also been evaluated using a universal material testing machine (Zwick/Roell Z020), as presented in **Figure S3(c)**. Apparently, even after being compressed for 15 cycles at a strain of 60%, PTGCA3 composite remains 86% of the first compressive stress, as high as 2058 kPa, indicating its excellent compression stability properties. Such good compression performance is believed to originate from the combination effect of highly-efficient 3D rGO/SWCNTs aerogel skeleton and the infiltrated flexible PDMS matrix.

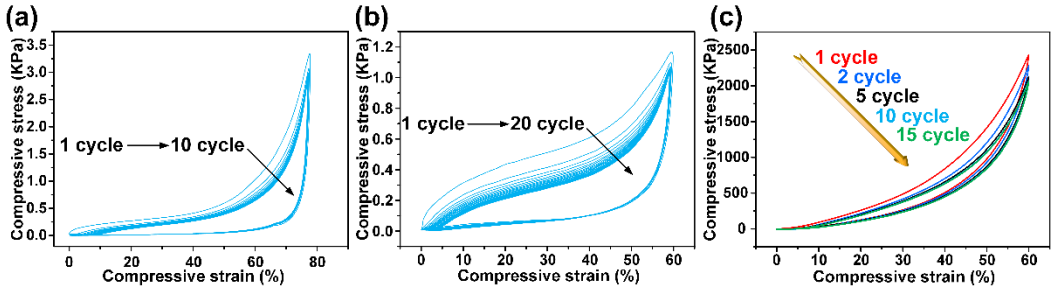

Figure S3. (a-b) Cyclic compressive stress-strain curves of TGCA3 aerogel at a maximal strain of 78% for 10 cycles (a) and at a strain of 60% for 20 cycles (b); (c) Cyclic compressive stress-strain curves of PTGCA3 composite at a stress strain of 60% for 15 cycles.

XPS C1S core level spectra analysis

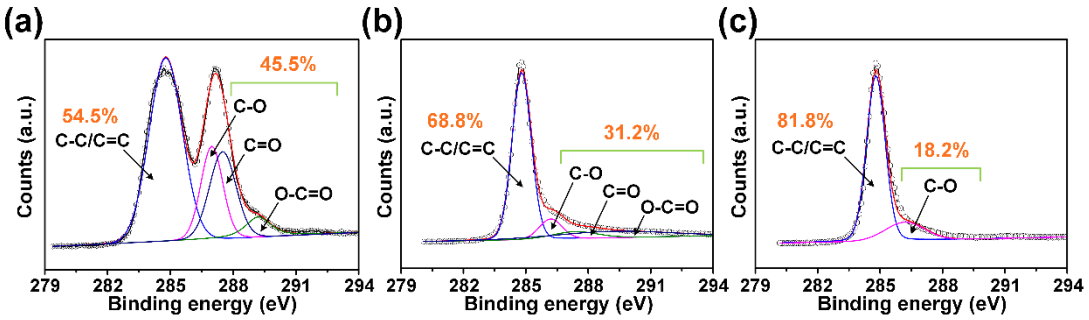

Figure S4. Fitted XPS spectra of C 1 s of GO (a), GCA3 (b), and TGCA3 (c).

To further ascertain the detailed evolution process of oxygenated functional groups in these materials, their XPS C 1s core level spectra are fitted into several typical deconvolution peaks using a sum of Lorentzian-Gaussian functions. As shown in **Figure S4a**, the XPS C 1s core level spectrum of GO is fitted with four typical characteristic peaks representing different chemical environments: C-C and C=C (sp^2 carbon, ~284.8 eV), epoxide/ether C-O (~287.0 eV), carbonyl C=O (~287.5 eV), and carboxyl O-C=O (~289.2 eV) groups. Meanwhile, the strength ratio of sp^2 carbon to total carbon constituent in GO have also been calculated and is determined to be 54.5%. In another word, about 45.5% of carbon atoms in GO component present an oxidized chemical state, such as C-O, C-O-C, and C=O groups. In comparison to GO, the C 1s spectrum of GCA3 also show four similar characteristic peaks (**Figure S4b**), however, the oxidizing functional groups ratio distinctly drops to 31.2%, demonstrating the efficient removal of oxygenated groups through the chemical reduction procedure via L-ascorbic acid. Moreover, there are only two fitted peaks in the C 1s core level spectrum of TGCA3 (**Figure S4c**), and thus the oxygenated groups content further greatly declines as low as 18.2%, which suggests the prominent elimination capacity toward oxygenating functional groups through the subsequent thermal annealing step.

XRD analysis

In addition, **Figure S5** shows XRD patterns of the materials. For SWCNT, two typical intense crystalline peaks are observed at 2θ = 21.1°, 43.2°, indicating its high crystallinity of SWCNT after heat treatment. GO exhibits a strong peak at 11.3°, which is due to the high oxidation of graphite by intercalation of oxygen-containing groups. However, GCA3 shows a broad peak at around 20.5°, indicating the chemical reduction of GO during the sol-gel self-assembly process. Compared with GCA3, after further thermal reduction treatment, TGCA3 exhibits a much narrower diffraction peak at ~22°, suggesting a higher degree of graphitization.

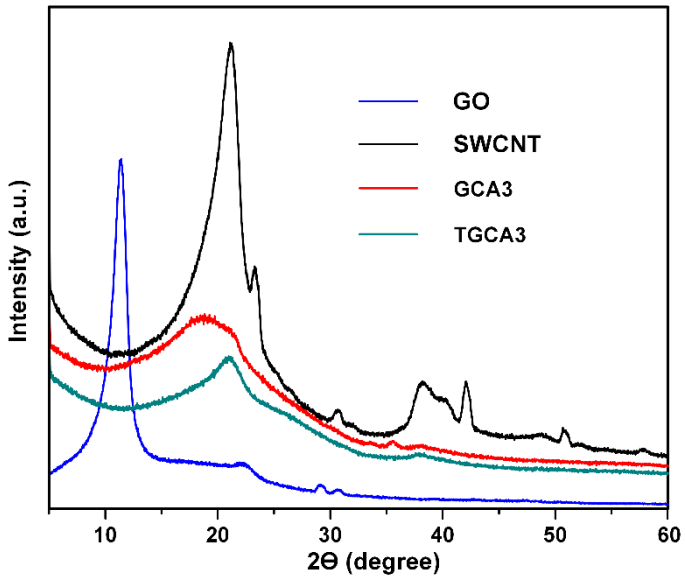

Figure S5. XRD patterns of GO, SWCNT, GCA3, and TGCA3.

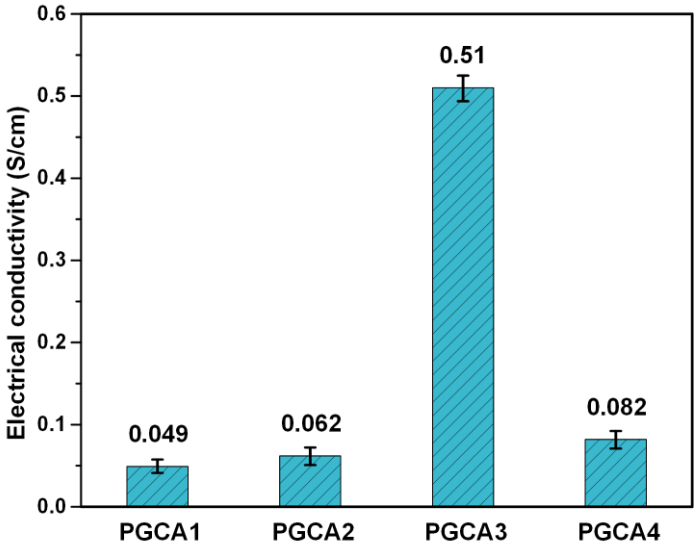

Figure S6. Electrical conductivities of PDMS composites reinforced with GCAx (x=1, 2, 3, 4).

EMI SE performance of TGCA aerogels

As can be seen from the **Figure S7**, the EMI SE values of TGCA3 and TGCA4 aerogels with the thickness of 1 mm are around 23.5 dB and 22 dB, respectively. It is well known that the EMI shielding effectiveness increases with increasing specimen thickness (Advanced Materials, 2013. 25(9), 1296-1300; Advanced Functional Materials, 2016. 26(3), 447-455). Thus, if the sample thickness of our pure TGCA aerogels (especially TGCA3) is increased to 2 mm, it can acquire an improved EMI SE of around 30 dB, which is approximately equal to the SE value of corresponding PDMS composite (PTGCA3, ~2 mm, see in **Figure 6**). Consequently, we can conclude that the conductive TGCA aerogels play a decisive role on the EMI SE performance of the PDMS nanocomposites. Such result can be explained by the fact that the 3D rGO/SWCNTs aerogel is the dominating contributor for the electrical conductivity of the PDMS composites.

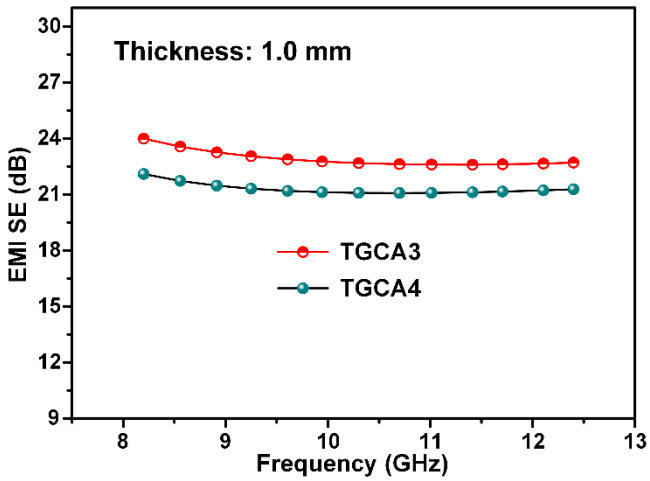

Figure S7. Plots of EMI SE versus frequency for TGCA3 and TGCA4 aerogels.

Table S1. Comparisons of EMI shielding performance and electrical properties of different carbon-based fillers/polymer nanocomposites.

Nanocomposites	Preparation methods	Filler Content (wt%)	Thickness (mm)	SEI SE (dB)	SSE[a] (dB/unit wt%)	Frequency (GHz)	Conducti -vity (S/cm)	Ref.
PS/rGO	Blending	~7.0	~2.5	~45.1	6.4	8.2-12.4	NG[b]	1
Epoxy/Graphene	Blending	~15	NG	~21	1.4	8.2-12.4	0.1	2
PEI/GF[c]	Blending	~10	~2.3	~20	2.0	8.2-12.4	$1E^{-6}$	3
PDMS/GF	CVD-backfilling	~0.8	2.0	~27	33.8	8.2-12.4	2.0	4
Epoxy/GF	CVD-backfilling	0.2	NG	NG	NG	NG	3.0	5
PU/rGO foam	Dip-coating	10	~20	19.9	2.0	8.2-12.4	$6E^{-4}$	6
Epoxy/SWCNT	Blending	15	1.5	15-20	1.3	0.5-1.5	0.2	7
CNT/PS foam	Blending	7	NG	19	2.7	8.2-12.4	NG	8
PE/CNT	Blending	5	2.1	46.4	9.3	8.2-12.4	0.56	9
PES/MWCNT[d]	Casting	20	0.5	35	1.8	8.2-12.4	4.5	10
Epoxy/CNT	Backfilling	~0.66	2.0	33.0	50.0	8.2-12.4	~1.5	11
GF/CNT/PDMS	CVD-backfilling	4.7	1.6	75	16.0	8.2-12.4	31.5	12
SEBS/GnP/CNT[e]	Blending	10	2.0	23.3	2.3	8.2-12.4	1.4	13
CPE[f]/MWCNT	Blending	15	2.0	36	2.4	8.2–12.4	$3.5\ E^{-3}$	14
CPE/carbon black	Melt mixing	40	0.56	42.4	1.1	8.2–12.4	$1E^{-3}$	15
CPE/CNF	Melt mixing	10	1.0	22.5	2.3	8.2–12.4	$1E^{-6}$	16
EMA/IRGO[g]	Melt blending	5	~1.8	~30	6.0	8.2–12.4	$8.2\ E^{-5}$	17
EMA/KCB[h]	Solution mixing	20	2.0	33.9	1.7	8.2–12.4	$1.4\ E^{-2}$	18
CPE/KCB	Solution mixing	30	1.0	38.4	1.3	8.2–12.4	$5\ E^{-2}$	19
PTGCA1	Backfilling	0.25	2.0	27.3	109.2	8.2~12.4	0.18	This work
PTGCA3	Backfilling	0.28	2.0	31.0	110.7	8.2~12.4	1.2	This work

[a]Specific SE value; [b]NG: not given; [c]GF: graphene foam; [d]PES: polyethersulfone;

[e]SEBS: poly (styrene-b-ethylene-ran-butylene-b-styrene), GnP: Graphene nanoplatelets;

[f]CPE: chlorinated polyethylene;

[g]EMA: ethylene methyl acrylate, IRGO: *in-situ* reduced graphene oxide;

[h]KCB: Ketjen carbon black;

References:

(1) Yan, D.; Pang, H.; Li, B.; Vajtai, R.; Xu, L.; Ren, P.; Wang, J.; Li, Z. Structured Reduced Graphene Oxide/Polymer Composites for Ultra-Efficient Electromagnetic Interference Shielding. *Adv. Funct. Mater.* **2015**, *25*, 559-566.

(2) Liang, J.; Wang, Y.; Huang, Y.; Ma, Y.; Liu, Z.; Cai, J.; Zhang, C.; Gao, H.; Chen, Y. Electromagnetic Interference Shielding of Graphene/Epoxy Composites. *Carbon* **2009**, *47*, 922-925.

(3) Ling, J.; Zhai, W.; Feng, W.; Shen, B.; Zhang, J.; Zheng, W. G. Facile Preparation of Lightweight Microcellular Polyetherimide/Graphene Composite Foams for Electromagnetic Interference Shielding. *ACS Appl. Mater. Inter.* **2013**, *5*, 2677-2684.

(4) Chen, Z.; Xu, C.; Ma, C.; Ren, W.; Cheng, H. Lightweight and Flexible Graphene Foam Composites for High-Performance Electromagnetic Interference Shielding. *Adv. Mater.* **2013**, *25*, 1296-1300.

(5) Jia, J.; Sun, X.; Lin, X.; Shen, X.; Mai, Y.; Kim, J. Exceptional Electrical Conductivity and Fracture Resistance of 3D Interconnected Graphene Foam/Epoxy Composites. *ACS Nano* **2014**, *8*, 5774-5783.

(6) Shen, B.; Li, Y.; Zhai, W.; Zheng, W. Compressible Graphene-Coated Polymer Foams with Ultralow Density for Adjustable Electromagnetic Interference (EMI) Shielding. *ACS Appl. Mater. Inter.* **2016**, *8*, 8050-8057.

(7) Li, N.; Huang, Y.; Du, F.; He, X.; Lin, X.; Gao, H.; Ma, Y.; Li, F.; Chen, Y.; Eklund, P. C. Electromagnetic Interference (EMI) Shielding of Single-Walled Carbon Nanotube Epoxy Composites. *Nano Lett.* **2006**, *6*, 1141-1145.

(8) Yang, Y.; Gupta, M. C.; Dudley, K. L.; Lawrence, R. W. Novel Carbon Nanotube-Polystyrene

Foam Composites for Electromagnetic Interference Shielding. *Nano Lett.* **2005**, *5*, 2131-2134.

(9) Jia, L.; Yan, D.; Cui, C.; Jiang, X.; Ji, X.; Li, Z. Electrically Conductive and Electromagnetic Interference Shielding of Polyethylene Composites with Devisable Carbon Nanotube Networks. *J. Mater. Chem. C* **2015**, *3*, 9369-9378.

(10) Abbas, N.; Kim, H. T. Multi-walled Carbon Nanotube/Polyethersulfone Nanocomposites for Enhanced Electrical Conductivity, Dielectric Properties and Efficient Electromagnetic Interference Shielding at Low Thickness. *Macromol. Res.* **2016**, *24*, 1084-1090.

(11) Chen, Y.; Zhang, H.; Yang, Y.; Wang, M.; Cao, A.; Yu, Z. High-Performance Epoxy Nanocomposites Reinforced with Three-Dimensional Carbon Nanotube Sponge for Electromagnetic Interference Shielding. *Adv. Funct. Mater.* **2016**, *26*, 447-455.

(12) Sun, X.; Liu, X.; Shen, X.; Wu, Y.; Wang, Z.; Kim, J. Graphene Foam/Carbon Nanotube/Poly(dimethyl siloxane) Composites for Exceptional Microwave Shielding. *Compos. Part A-Appl. S.* **2017**, *92*, 190-197.

(13) Kuester, S.; Demarquette, N. R.; Ferreira, J. C.; Soares, B. G.; Barra, G. M. O. Hybrid Nanocomposites of Thermoplastic Elastomer and Carbon Nanoadditives for Electromagnetic Shielding. *Eur. Polym. J.* **2017**, *88*, 328-339.

(14) Mondal, S.; Das, P.; Ganguly, S.; Ravindren, R.; Remanan, S.; Bhawal, P.; Das, T. K.; Das, N. C. Thermal-Air Ageing Treatment on Mechanical, Electrical, and Electromagnetic Interference Shielding Properties of Lightweight Carbon Nanotube Based Polymer Nanocomposites. *Composites Part A: Applied Science and Manufacturing* **2018**, *107*, 447-460.

(15) Mondal, S.; Ganguly, S.; Das, P.; Bhawal, P.; Das, T. K.; Ravindren, R.; Ghosh, S.; Das, N. C. Effect of Thermal-Air Ageing Treatment on Mechanical Properties and Electromagnetic Interference

Shielding Effectiveness of Low-Cost Nano-Structured Carbon Filled Chlorinated Polyethylene. *Mater. Sci. Eng., B* **2017**, *225*, 140-149.

(16) Mondal, S.; Nayak, L.; Rahaman, M.; Aldalbahi, A.; Chaki, T. K.; Khastgir, D.; Das, N. C. An Effective Strategy to Enhance Mechanical, Electrical, and Electromagnetic Shielding Effectiveness of Chlorinated Polyethylene-Carbon Nanofiber Nanocomposites. *Compos. Part B:Eng.* **2017**, *109*, 155-169.

(17) Bhawal, P.; Ganguly, S.; Das, T. K.; Mondal, S.; Choudhury, S.; Das, N. C. Superior Electromagnetic Interference Shielding Effectiveness and Electro-Mechanical Properties of EMA-IRGO Nanocomposites through the in-situ Reduction of GO from Melt Blended EMA-GO Composites. *Compos. Part B:Eng.* **2018**, *134*, 46-60.

(18) Mondal, S.; Ganguly, S.; Das, P.; Khastgir, D.; Das, N. C. Low Percolation Threshold and Electromagnetic Shielding Effectiveness of Nano-Structured Carbon Based Ethylene Methyl Acrylate Nanocomposites. *Compos. Part B:Eng.* **2017**, *119*, 41-56.

(19) Mondal, S.; Ganguly, S.; Rahaman, M.; Aldalbahi, A.; Chaki, T. K.; Khastgir, D.; Das, N. C. A Strategy to Achieve Enhanced Electromagnetic Interference Shielding at Low Concentration with a New Generation of Conductive Carbon Black in a Chlorinated Polyethylene Elastomeric Matrix. *Phys. Chem. Chem. Phys.* **2016**, *18*, 24591-24599.